Coupled free vibrations of liquid in a three-dimensional rectangular container with an elastic cover
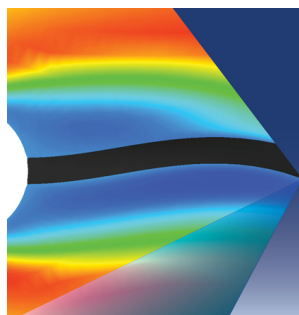
K. Ren (ID) ; G. X. Wu ✉ (ID) ; Y. F. Yang

Check for updates

View Online   Export Citation

Physics of Fluids

Special Topic:

Fluid-Structure Interaction

Guest Editors: A-Man Zhang, Tiegang Liu, Boo Cheong Khoo and Nhan Phan-Thien

Submit Today!

AIP Publishing

Coupled free vibrations of liquid in a three-dimensional rectangular container with an elastic cover

View Online   Export Citation   CrossMark

K. Ren, (iD) G. X. Wu,[a] (iD) and Y. F. Yang

AFFILIATIONS

Department of Mechanical Engineering, University College London, Torrington Place, London WC1E 7JE, United Kingdom

[a]Author to whom correspondence should be addressed: g.wu@ucl.ac.uk

ABSTRACT

The coupled free vibration of liquid and its elastic cover, such as a plate or a membrane, in a three-dimensional rectangular tank is investigated through an analytical scheme based on the velocity potential theory for the flow and the linear elastic theory for the cover. For the fluid domain, the velocity potential is expanded into double cosine series along the longitudinal and transverse directions, respectively, with the corresponding eigenvalues determined from the impermeable conditions on the side walls. The vertical modes of the potential are obtained from the Laplace equation. The deflection of the rectangular cover is expanded into the same double cosine series to match the potential, together with additional terms for satisfying the edge conditions. The polynomials are used for these additional terms, which are then expanded into cosine series. For the expansions of the higher-order derivatives of the deflection, the derivatives of these polynomial terms are expanded into cosine series directly, rather than being obtained through differentiating the cosine series of the deflection, to avoid the non-convergent series. Through imposing the boundary conditions on the fluid–plate interface and edge conditions, an infinite matrix equation for the unknown coefficients can be established. The natural frequencies can be obtained when the determinant of the matrix is zero. In practical computation, the infinite matrix equation is truncated into finite size. Results are first provided for natural frequencies. This is followed by the corresponding natural mode shapes and principal strains distribution on the cover. The underlying physics of these results is then provided.

I. INTRODUCTION

The motion of liquid inside a tank or container, which is also named as sloshing, has received extensive study as it can be commonly seen in nature and has a wide range of engineering applications. Sloshing may occur in lakes, reservoirs, harbors, and bays, referred to as seiches,[1] due to some environmental excitation such as winds and earthquakes. In marine engineering, sloshing can occur in a tank of a ship containing liquid, for example, during its transportation of the liquified natural gas (LNG) and other types of liquid fuels such as liquid hydrogen (LH$_2$). Violent motion of liquid inside the tank can be excited by the motion of the ship, especially when the oscillation frequency of the ship is close to one of the natural frequencies of the tank. This may have severe adverse effects on the ship stability, also induce large impact loads, and cause structural damage to the tank. On the other hand, sloshing can be used beneficially through anti-rolling tanks installed in ships to provide a moment to counter that

due to wave excitation.[2] In addition, during transportation of liquefied fuels by ships or trucks, one of the main challenges is the potential boiloff, which can be caused through evaporation of liquid fuels. Excessive boiloff gas may influence the operating pressure in the container and risk the safe transportation. The liquid sloshing in tanks can affect the rate of boiloff through the heat and mass transfer between liquid and vapor.[3] There are many other areas where sloshing can be important. For example, sloshing also occurs in the liquid-propellant container of spacecraft[4] and aircraft[5] and in the fuel tank of other vehicles such as automobiles.[6] Furthermore, tuned liquid dampers (TLD) have been widely used in high-rise buildings to dampen the wind-induced vibration.[7]

The literature on free surface sloshing modeling based on different governing equations such as the Navier–Stokes (NS) equations and Laplace equation has been summarized in Ibrahim[8] and Faltinsen and Timokha.[9] In particular, there is an extensive amount of work on

21 August 2024 09:24:30

free surface sloshing in a three-dimensional (3D) rectangular tank due to the practical importance. Based on the velocity potential flow theory, an analytical solution for small amplitude motions was given by Abramson.[10] For large amplitude motions, Wu et al.[11] developed a fully nonlinear finite element method and obtained the solution numerically, and Faltinsen et al.[12] obtained the solutions based on the multimodal approach. Based on the viscous theory, one of the examples is that by Liu and Lin,[13] where NS equations were solved numerically together with the large eddy simulation, and the volume of fluid method was used to track the interface of liquid and air. Apart from numerical simulation, experimental studies have also been widely undertaken for liquid sloshing in tanks, such as Caron et al.[14] for a circular cylindrical tank, Núñez Aedo et al.[15] for a rectangular tank, and Zhang et al.[16] for a floating rectangular tank in water waves.

Resonant sloshing in a container occurs when the excitation frequency is close to one of the natural frequencies of the tank. When damping is also small, resonant motion can be exceedingly large. In many cases, a tank can be characterized as a clean tank, and the viscous damping is small.[9] Therefore, one of the optimal sloshing suppression strategies is to shift the natural frequencies of the tank away from the range of excitation frequencies. Structures such as baffles and elastic floating covers are commonly designed and installed in containers. For example, a recent work done by Kuznetsov and Motygin[17] considered the effect of radial baffles to the liquid sloshing in an upright circular container. In addition, active sloshing control has also been proposed based on these structures, such as in Hernández and Santamarina,[18] Hasheminejad et al.,[19] and Xie and Zhao.[20] Among many options, one of them is to use an elastic thin cover on the liquid surface. Thus, understanding the effect of the elastic cover on sloshing is of important practical relevance. The cover may be an elastic membrane and an elastic plate. Bauer[21] considered the free vibration of liquid in a circular tank completely covered by an elastic membrane or a plate based on the Bessel-Fourier series expansion. A 2D rectangular tank with membrane cover was considered by Parasil and Watanabe,[22] where the effect of nonlinearity was included. Using a similar method as in Bauer,[21] Bauer and Komatsu[23] further investigated a circular tank covered by a doughnut-shaped elastic plate, which covers the liquid surface partially, with the inner circular area of the liquid surface being free. The problem was reconsidered by Kim and Lee[24] using the Rayleigh-Ritz method. For the case where a circular plate concentrically covers the free liquid surface, while the outer liquid surface of a circular cylindrical container remains free, Amabili[25] obtained the frequencies of the free vibration by using the Rayleigh-Ritz method. Recently, Ren et al.[26] developed two different efficient methods for the circular tank. Various edge conditions were considered. Extensive results were provided for natural frequencies, modal shapes, and maximum principal strain. A related problem of sloshing in cylindrical storage tanks under seismic excitation was considered by Matsui.[27]

The works mentioned above are all a circular tank with an elastic cover. There is little work on a rectangular tank based on analytical or semi-analytical procedure. This will, therefore, be considered in the present work. The free vibration of the coupled system of liquid and an elastic cover will be studied through an analytical scheme based on the linearized velocity potential flow theory and the Kirchhoff-Love thin plate theory. It is worth mentioning here that different from the free surface sloshing, some additional challenges exist in this coupled fluid-plate problem. One is the higher-order derivative term in the

dynamic condition of the elastic plate, and another one is due to the treatment of various edge conditions. In this work, an analytical scheme applicable for various edge conditions has been developed, which allows us to investigate their influence in a much more convenient way. It should be mentioned that the present problem and scheme are very much different from those of a circular tank. Physically for the circular tank, there is no coupling among different circumferential modes in commonly adopted edge conditions, or, clamped, fixed and free. For the rectangular tank, the modes are usually coupled. Mathematically, as the solutions in both cases are based on analytical procedure, the method and derivation are very different. An obvious difference is that in the horizontal plane, one is done in the polar coordinate system, while the other is done in the Cartesian coordinate system. More importantly, for the circular tank, both the potential and the cover deflection are expanded into Fourier and Bessel series. The expansions of the cover deflection and its derivatives are linked through integration by parts. However, this method cannot be used for the rectangular plate, and thus, a different method is used. The potential is expanded into cosine series in the horizontal directions. The cover deflection is expanded similarly. To meet the edge conditions, four additional terms are introduced in each direction in the cover deflection. Without loss of generality, polynomial functions are used. For the circular tank, the natural frequencies can be obtained from the roots of an infinite summation, which is truncated. For the rectangular tank, they are obtained when the determinant of an infinite matrix is zero, which is truncated at a sufficiently large number. However, when the size of the matrix increases, direct computation of the determinant becomes impractical. A Gaussian elimination scheme is then used to search for the natural frequencies. Extensive results are provided for natural frequencies, mode shapes, and maximum principal strain.

The paper is organized as follows. In Sec. II, the mathematical model and solution procedure are introduced. Detailed results and discussion on the natural frequencies, mode shapes, and principal strain are, respectively, provided in Secs. III–V. Finally, conclusions are drawn in Sec. VI.

II. MATHEMATICAL MODEL AND SOLUTION PROCEDURES

We consider the problem of free sloshing motion of liquid in a three-dimensional rectangular tank of rigid side walls with an elastic cover. The sketch of this problem is shown in Fig. 1. A fixed Cartesian coordinate system is established on the tank with the origin located on the center point of the undisturbed plane of the cover, with its z-axis pointing vertically upward. The half length and width of the tank are denoted as l and b, with their directions along the x- and y-axes, respectively. The depth of the liquid is H.

The velocity potential theory is adopted for fluid motion, while the Kirchhoff-Love plate theory is adopted for the elastic cover in the mathematical modeling. Based on the assumption that the liquid in the tank is incompressible, the velocity potential Φ satisfies the Laplace equation:

$$\frac{\partial^2 \Phi}{\partial x^2} + \frac{\partial^2 \Phi}{\partial y^2} + \frac{\partial^2 \Phi}{\partial z^2} = 0. \tag{1}$$

We assume that there is no gap between fluid and the elastic cover. The dynamic condition on the interface of liquid domain and the elastic plate can be given as
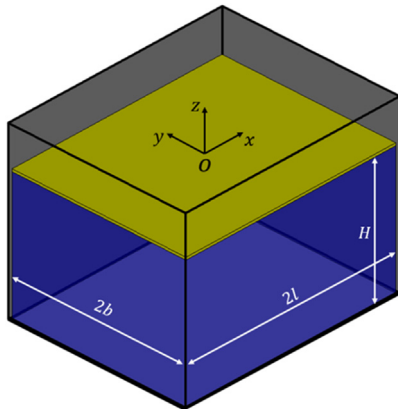
FIG. 1. The sketch of the problem.

$$\rho_e h \frac{\partial^2 W}{\partial t^2} + L\nabla^4 W = -\rho\Phi_t - \rho g W \quad (z=0), \tag{2}$$

where W is the deflection of the elastic plate, t is the time, ρ is the density of liquid, g is the gravitational acceleration, and $L = Eh^3/[12(1-\nu^2)]$, E, h, ρ_e, and ν are, respectively, the flexural rigidity, Young's modulus, thickness, density, and Poisson's ratio of the plate. $\nabla^4 = \nabla^2\nabla^2$ is the biharmonic differential operator. The right-hand side of Eq. (2) is the fluid pressure acting on the elastic cover, which is obtained from the linearized Bernoulli equation. For a membrane, the term of $L\nabla^4 W$ in Eq. (2) should be replaced by $T\nabla^2 W$, where T is the tension. Without loss of generality, the derivation and results below will focus on the plate.

The linearized kinematic condition at the interface can be given as

$$\frac{\partial W}{\partial t} = \frac{\partial \Phi}{\partial z}, \quad (z=0). \tag{3}$$

On the rigid side walls and bottom of the tank, we have the impermeable boundary conditions as

$$\left.\frac{\partial \Phi}{\partial x}\right|_{x=\pm l} = \left.\frac{\partial \Phi}{\partial y}\right|_{y=\pm b} = \left.\frac{\partial \Phi}{\partial z}\right|_{z=-H} = 0. \tag{4}$$

In addition, the boundary conditions for plate edges must be imposed. The most commonly used types are clamped, free, and simply supported edges. On the edge of $x = \pm l$, we have

$$W(x = \pm l) = 0, \tag{5a}$$
$$W_x(x = \pm l) = 0, \tag{5b}$$

for clamped edge

$$\left(\frac{\partial^2 W}{\partial x^2} + \nu\frac{\partial^2 W}{\partial y^2}\right)_{x=\pm l} = 0, \tag{6a}$$

$$\left(\frac{\partial^3 W}{\partial x^3} + (2-\nu)\frac{\partial^3 W}{\partial x\partial y^2}\right)_{x=\pm l} = 0, \tag{6b}$$

for free edge, and

$$W(x = \pm l) = 0, \tag{7a}$$

$$\left(\frac{\partial^2 W}{\partial x^2} + \nu\frac{\partial^2 W}{\partial y^2}\right)_{x=\pm l} = 0, \tag{7b}$$

for simply supported edge.[29] For the other pair of edges at $y = \pm b$, the corresponding equations for the edge conditions can be obtained from Eqs. (5) to (7) by simply exchanging x and y. For the free corner formed by two free edges, the condition $\frac{\partial^2 w}{\partial x\partial y} = 0$ should be also satisfied.[29,30]

To investigate the free vibration of the system, we may write $\Phi = \text{Re}\{\phi \times e^{-i\omega t}\}$ and $W = \text{Re}\{w \times e^{-i\omega t}\}$, where ω is a natural frequency of the system and $i = \sqrt{-1}$ is the imaginary unit. Taking into account Eq. (4), expanding ϕ into cosine series in x and y directions and then solving ordinary differential equation in the z direction, we can write the solution of ϕ as

$$\phi = \sum_{m=0}^{\infty}\sum_{n=0}^{\infty} \mathcal{P}_{mn} \cos a_m(x+l) \cos b_n(y+b) \frac{\cosh k_{mn}(z+H)}{\cosh k_{mn}H} \tag{8}$$

where

$$a_m = \frac{m\pi}{2l}, \quad b_n = \frac{n\pi}{2b}, \quad k_{mn}^2 = a_m^2 + b_n^2.$$

By substituting Eq. (8) into the dynamic equation of the plate, we have

$$L\nabla^4 w + (\rho g - \rho_e h\omega^2) w$$
$$= i\rho\omega \sum_{n=0}^{\infty}\sum_{m=0}^{\infty} \mathcal{P}_{mn} \cos a_m(x+l) \cos b_n(y+b). \tag{9}$$

The solution of w may be written as

$$w = w_0 + w_1 + w_2. \tag{10}$$

Here, w_0 can be written in the form of double series, given the right-hand side of Eq. (9)

$$w_0 = \sum_{n=0}^{\infty}\sum_{m=0}^{\infty} C_{mn} \cos a_m(x+l) \cos b_n(y+b), \tag{11}$$

and w_1 and w_2 in Eq. (10) are introduced to account for edge conditions at $x = \pm l$ and $y = \pm b$, respectively. We may write w_1 in the following form:

$$w_1 = \sum_{n=0}^{\infty} \cos b_n(y+b) \cdot f_n(x). \tag{12}$$

We notice that the edge conditions in Eqs. (5)–(7) have two conditions on each side and four in total, involving derivatives up to third order. Taking this account, we may write

$$f_n(x) = d_n^{(1)}\left(\frac{x}{l}\right) + d_n^{(2)}\left(\frac{x}{l}\right)^2 + d_n^{(3)}\left(\frac{x}{l}\right)^3 + d_n^{(4)}\left(\frac{x}{l}\right)^4. \tag{13}$$

Similarly, we may write w_2 as

$$w_2 = \sum_{m=0}^{\infty} \cos a_m(x+l) \cdot g_m(y), \tag{14}$$

with

$$g_m(y) = c_m^{(1)}\left(\frac{y}{b}\right) + c_m^{(2)}\left(\frac{y}{b}\right)^2 + c_m^{(3)}\left(\frac{y}{b}\right)^3 + c_m^{(4)}\left(\frac{y}{b}\right)^4. \tag{15}$$

In this way, the satisfaction of the governing equation is taken care of by C_{mn} in Eq. (11), edge conditions at $x = \pm l$ by $d_n^{(i)}$, $i = 1, 2, 3$, and 4 in Eq. (13), and edge conditions by $c_m^{(i)}$, $i = 1, 2, 3$, and 4 in Eq. (15), while they are all coupled. Then, w can then be written as

$$w = \sum_{n=0}^{\infty}\sum_{m=0}^{\infty} C_{mn} \times \cos a_m(x + l)\cos b_n(y + b)$$
$$+ \sum_{n=0}^{\infty}\cos b_n(y + b)\cdot f_n(x) + \sum_{m=0}^{\infty}\cos a_m(x + l)\cdot g_m(y). \tag{16}$$

Here, we may notice that w in Eq. (16) is similar to that in Li $et\ al.$[31] for a plate without liquid, where a different procedure is followed.

We may expand $\left(\frac{x}{l}\right)^i$ and $\left(\frac{y}{b}\right)^i$ $(i = 0 \sim 4)$ into following series:

$$\left(\frac{x}{l}\right)^i = \sum_{m=0}^{\infty}\mu_m^{(i)}\cos a_m(x + l), \tag{17}$$

$$\left(\frac{y}{b}\right)^i = \sum_{n=0}^{\infty}\mu_n^{(i)}\cos b_n(y + b), \tag{18}$$

where $\mu_n^{(0)} = \delta_{n0}$ and

$$\mu_n^{(1)} = \begin{cases} 0, & n = 0, \\ \dfrac{4(-1 + (-1)^n)}{n^2\pi^2}, & n > 0, \end{cases}$$

$$\mu_n^{(2)} = \begin{cases} 1/3, & n = 0, \\ \dfrac{8(1 + (-1)^n)}{n^2\pi^2}, & n > 0, \end{cases}$$

$$\mu_n^{(3)} = \begin{cases} 0, & n = 0, \\ \dfrac{12(n^2\pi^2 - 8)(-1 + (-1)^n)}{n^4\pi^4}, & n > 0, \end{cases}$$

$$\mu_n^{(4)} = \begin{cases} 1/5, & n = 0, \\ \dfrac{16(n^2\pi^2 - 24)(1 + (-1)^n)}{n^4\pi^4}, & n > 0. \end{cases}$$

Substituting Eqs. (16)–(18) into (9), then based on the orthogonality of the trigonometric functions, we have

$$\sum_{i=1}^{4}\left(\alpha_{mn}^{(i)}c_m^{(i)} + \beta_{mn}^{(i)}d_n^{(i)}\right) = S_{mn}C_{mn} + i\rho\omega\mathcal{P}_{mn}$$
$$(m, n = 0, 1, 2, 3, \ldots), \tag{19}$$

where

$$S_{mn} = -\left[L(a_m^2 + b_n^2)^2 + \rho g - \rho_e h\omega^2\right], \tag{20}$$

$$\alpha_{mn}^{(i)} = (La_m^4 + \rho g - \rho_e h\omega^2)\mu_n^{(i)} - \frac{4La_m^2}{b^2}\delta_{n0}\delta_{i2}$$
$$- \frac{12La_m^2}{b^2}\mu_n^{(1)}\delta_{i3} + \left(\frac{24L}{b^4}\delta_{n0} - \frac{24La_m^2}{b^2}\mu_n^{(2)}\right)\delta_{i4}$$
$$= -S_{m0}\mu_n^{(i)} + \frac{24L}{b^4}\delta_{n0}\delta_{i4} - \frac{2a_m^2 L \times i(i-1)\mu_n^{(i-2)}}{b^2}, \tag{21}$$

$$\beta_{mn}^{(i)} = (Lb_n^4 + \rho g - \rho_e h\omega^2)\mu_m^{(i)} - \frac{4Lb_n^2}{l^2}\delta_{m0}\delta_{i2}$$
$$- \frac{12Lb_n^2}{l^2}\mu_m^{(1)}\delta_{i3} + \left(\frac{24L}{l^4}\delta_{m0} - \frac{24Lb_n^2}{l^2}\mu_m^{(2)}\right)\delta_{i4}$$
$$= -S_{0n}\mu_m^{(i)} + \frac{24L}{l^4}\delta_{m0}\delta_{i4} - \frac{2b_n^2 L \times i(i-1)\mu_m^{(i-2)}}{l^2}, \tag{22}$$

and δ_{ij} is the Kronecker delta function.

Here, we may notice that the expansions of the derivatives of $f(x)$ and $g(y)$ are obtained, respectively, from Eqs. (17) and (18) directly, rather than from the derivatives of their expansions, as the latter may lead to a non-convergent series.

The kinematic condition is

$$-i\omega w = \phi_z, \quad z = 0. \tag{23}$$

Substituting Eqs. (8), (13), (15), (16) into Eq. (23), and further based on the orthogonality of trigonometric functions, we have

$$-i\omega\left(\sum_{i=1}^{4}\mu_m^{(i)}d_n^{(i)} + \sum_{i=1}^{4}\mu_n^{(i)}c_m^{(i)}\right) = k_{mn}\tanh k_{mn}H\,\mathcal{P}_{mn} + i\omega C_{mn}.$$
$$(m, n = 0, 1, 2, 3\ldots). \tag{24}$$

From Eqs. (19) and (24), we can write $\mathcal{P}_{mn}$ and C_{mn} in terms of $c_m^{(i)}$ and $d_n^{(i)}$ as

$$\mathcal{P}_{mn} = -\frac{i\omega}{k_{mn}S_{mn}\tanh k_{mn}H + \rho\omega^2}$$
$$\times \sum_{i=1}^{4}\left[\left(S_{mn}\mu_m^{(i)} + \beta_{mn}^{(i)}\right)d_n^{(i)} + \left(S_{mn}\mu_n^{(i)} + \alpha_{mn}^{(i)}\right)c_m^{(i)}\right], \tag{25}$$

$$C_{mn} = -\frac{\rho\omega^2}{S_{mn}(k_{mn}S_{mn}\tanh k_{mn}H + \rho\omega^2)}$$
$$\times \sum_{i=1}^{4}\left[\left(S_{mn}\mu_m^{(i)} + \beta_{mn}^{(i)}\right)d_n^{(i)} + \left(S_{mn}\mu_n^{(i)} + \alpha_{mn}^{(i)}\right)c_m^{(i)}\right]$$
$$+ \frac{1}{S_{mn}}\sum_{i=1}^{4}\left(\alpha_{mn}^{(i)}c_m^{(i)} + \beta_{mn}^{(i)}d_n^{(i)}\right). \quad (m, n = 0, 1, 2, 3\ldots). \tag{26}$$

Apart from Eqs. (19) and (24), edge conditions also need to be imposed on w in Eq. (16). By using orthogonality of trigonometric functions and substituting the expressions of $\mathcal{P}_{mn}$ and C_{mn} in Eqs. (25) and (26), we can obtain systems of linear equations for unknowns $c_m^{(i)}$ and $d_n^{(i)}$ shown in various edge conditions of Appendixes. The matrix equation can be written as

$$A\cdot x = 0, \tag{27}$$

where x is a column vector, which can be written as

$$x = [c_0, c_1, \ldots, c_m, \ldots, d_0, d_1, \ldots, d_n, \ldots]^T,$$

with $c_m = (c_m^{(1)}, c_m^{(2)}, c_m^{(3)}, c_m^{(4)})$ and $d_n = (d_n^{(1)}, d_n^{(2)}, d_n^{(3)}, d_n^{(4)})$. The coefficients of matrix A in Eq. (27) can be obtained from individual equations in the Appendixes for each set of edge conditions. In practical calculation, truncations are made for m and n at $M - 1$ and $N - 1$, respectively.

The natural frequencies correspond to the roots of $\det\{A\} = 0$ or the values of ω^* at which the coefficient matrix is singular. As the size of matrix increases, direct computation of its determinant becomes impractical. To search for the roots of $\det\{A\} = 0$, we vary ω^* with a sufficiently small interval $\Delta\omega^*$. We then use the Gaussian elimination algorithm with column pivoting. When the Gaussian elimination reaches the k th row, column swapping is conducted to ensure the diagonal element to be the principal one. When the absolute value of the principal element is sufficiently small or is below a given small threshold value, then the matrix is regarded to be singular. To reduce the computational cost, we may investigate $\det\{A\} = 0$ directly for smaller M and N, which can give a good estimate for the positions of the solutions. Then, we can further use the Gaussian elimination near these points at larger M and N.

For cases with edge conditions of the same type on the four edges, we can further split the unknown $\boldsymbol{x}$ in Eq. (27) into four groups: (a) $c_{2m}^{(2i)}, d_{2n}^{(2i)}$; (b) $c_{2m}^{(2i-1)}, d_{2n+1}^{(2i)}$; (c) $c_{2m+1}^{(2i)}, d_{2n}^{(2i-1)}$, and (d) $c_{2m+1}^{(2i-1)}, d_{2n+1}^{(2i-1)}$ ($i = 1, 2$; $m, n = 0, 1, 2\ldots$), which, respectively, correspond to the symmetric–symmetric (S–S) modes, the symmetric–antisymmetric (S–A) modes, the antisymmetric–symmetric (A–S) modes, and the antisymmetric–antisymmetric (A–A) modes with respect to x and y axes. The detailed analysis for completely clamped edges can be seen in Appendix A, while the other two sets of edge conditions can be analyzed in a similar way. Therefore, the unknowns in each group are coupled with each other but are fully uncoupled with those in other three groups. In such cases, the natural frequencies in each group can be obtained from the solutions of the zero-determinant of the matrix corresponding to this group. For a square tank, it can be expected that the natural frequencies of the A–S mode are the same as those of S–A modes.

The free corner condition $w_{xy} = 0$ is satisfied automatically in the present procedure. Integrating the zero Kirchhoff shear force edge condition at $x = -l$ in Eq. (6) with respect to y from $-b$ to b, we have

$$\int_{-b}^{b}\left[\frac{\partial^3 w}{\partial x^3} + (2-\nu)\frac{\partial^3 w}{\partial x \partial y^2}\right]_{x=-l} dy$$
$$= \int_{-b}^{b}\frac{\partial^3 w}{\partial x^3}\bigg|_{x=-l} dy + (2-\nu)$$
$$\times \left[\frac{\partial^2 w}{\partial x \partial y}\bigg|_{x=-l,y=b} - \frac{\partial^2 w}{\partial x \partial y}\bigg|_{x=-l,y=-b}\right] = 0. \quad (28)$$

Using Eq. (10), for w_{xxx} with f_n''' being obtained directly from Eq. (13) and then (B.5) for $n = 0$, we obtain

$$\frac{\partial^2 w}{\partial x \partial y}\bigg|_{x=-l,y=b} - \frac{\partial^2 w}{\partial x \partial y}\bigg|_{x=-l,y=-b}$$
$$= -\frac{2b}{2-\nu}\times f_0'''(-l) = -\frac{2b\left(6d_0^{(3)} - 24d_0^{(4)}\right)}{(2-\nu)l^3} = 0. \quad (29)$$

In addition, multiply Eq. (6a) by $\cos b_1(y+b)$ first and then integrate as in Eq. (28). Using integration by parts twice for the second term, we have

$$\int_{-b}^{b}\left[\frac{\partial^3 w}{\partial x^3} + (2-\nu)\frac{\partial^3 w}{\partial x \partial y^2}\right]_{x=-l}\cos b_1(y+b)\,dy$$
$$= bf_1'''(-l) + (2-\nu)$$
$$\times \left\{\left[\cos b_1(y+b)\left(\frac{\partial^2 w}{\partial x \partial y}\right)_{x=-l}\right]_{-b}^{b} - bb_1^2 f_1'(-l)\right\} = 0, \quad (30)$$

or

$$[w_{xy}]_{x=-l,y=b} + [w_{xy}]_{x=-l,y=-b}$$
$$= \frac{b}{2-\nu}\times\left[f_1'''(-l) - (2-\nu)b_1^2 f_1'(-l)\right]$$
$$= \frac{b}{2-\nu}\left[\frac{(2-\nu)b_1^2}{l}\left(-d_1^{(1)} + 2d_1^{(2)} - 3d_1^{(3)} + 4d_1^{(4)}\right)\right.$$
$$\left. + \frac{6}{l^3}d_1^{(3)} - \frac{24}{l^3}d_1^{(4)}\right]. \quad (31)$$

By using Eq. (B.5) for $n = 1$, we can further have $w_{xy}|_{x=-l,y=b} + w_{xy}|_{x=-l,y=-b} = 0$. Therefore, we have $w_{xy}|_{x=-l,y=b} = w_{xy}|_{x=-l,y=-b} = 0$ when free edge conditions are imposed in the Appendix of the present procedure. Similar operation can be applied other free edges, and therefore, we have on all the four corners, or $w_{xy}|_{x=\pm l,y=\pm b} = 0$.

III. NATURAL FREQUENCIES

A. Natural frequencies of a rectangular plate without liquid

When there is no liquid beneath the elastic plate, the rectangular plate is vibrating in the vacuum. In such a case, $\rho = 0$ can be taken in all the above equations. The solution may be compared with existing results, such as those provided by Leissa,[30] to verify the present procedure. The threshold value used in the Gaussian elimination is chosen as 10^{-4}. In Table I–III, we give the present results and those from Leissa[30] of the six lowest natural frequencies at three different combinations of edge conditions on the four edges, namely, completely clamped edges (*C-C-C-C*), completely free edges (*F-F-F-F*), and one clamped, one simply supported, and two neighboring free edges (*C-SS-F-F*). The case with the aspect ratio $l/b = 1.5$ is used as an example.

TABLE I. Natural frequency parameters $(\lambda = 4l^2\omega\sqrt{\rho_e h/L})$ for completely clamped edges (*C-C-C-C*), $(\nu = 0.3)$.

Frequency sequence	Leissa[30]	Present results		
		$M = N = 10$	$M = N = 15$	$M = N = 20$
1	60.772	60.757	60.761	60.761
2	93.860	93.821	93.831	93.833
3	148.82	148.76	148.78	148.78
4	149.74	149.64	149.67	149.67
5	179.66	179.51	179.55	179.56
6	226.92	226.78	226.81	226.82

TABLE II. Natural frequency parameters ($\lambda = 4l^2\omega\sqrt{\rho_e h/L}$) for completely free edges (*F-F-F-F*), ($\nu = 0.3$).

Frequency sequence	Leissa[30]	Present results		
		$M = N = 10$	$M = N = 15$	$M = N = 20$
1	20.128	20.101	20.097	20.096
2	21.603	21.431	21.417	21.415
3	46.654	46.393	46.358	46.352
4	50.293	49.952	49.919	49.915
5	58.201	57.814	57.748	57.726
6	67.494	67.096	67.050	67.038

In above tables, it can be observed that convergence with N and M has been achieved for the present results, especially the maximum relative error between results at $N = M = 15$ and $N = M = 20$ is smaller than 0.05%. A very good agreement between the present results and those in Leissa[30] can also be seen.

It may seem that by simply taking liquid density $\rho \to 0$ in the solution procedure in Sec. II, the result will be identical to that of $\rho = 0$, or the free vibration of a rectangular plate in the vacuum. However, as it can be seen in Appendixes, the equations may not reduce to those for a rectangular plate in the vacuum. In fact, we may consider the term $\frac{k_{mn}\tanh k_{mn}H}{S_{mn}k_{mn}\tanh k_{mn}H + \rho\omega^2}$. At $m = n = 0$, this is always zero when ρ tends to zero but is not equal to zero. It becomes non-zero when $\rho = 0$. This kind of difference may affect the results of ω^*, which depends on the edge conditions. For *C-C-C-C* conditions, it is noticed that some frequencies at $\rho \to 0$ are the same as those at $\rho = 0$, and others are not. As $m = n = 0$ belongs to the S-S modes, only the natural frequencies corresponding to S-S modes are affected, while others are not. For *F-F-F-F* edge conditions, as shown in B1–B4 in Appendix B, there is always a factor $(a_m^2 + \nu b_n^2)$ in the series, which equals zero at $m = n = 0$. Therefore, the coefficient matrix will always be the same for both $\rho \to 0$ and $\rho = 0$, so as the solutions of ω^*.

Physically, when $\rho \to 0$, the dynamic effect of the liquid on the plate will disappear, or the right-hand side of Eq. (2) will be zero. However, the kinematic condition in Eq. (3) remains. As the integration of the normal derivative of the potential, $\partial\phi/\partial n$, over the fluid boundary must be zero due to mass continuity, or the Laplace equation, the integration of the right-hand side of Eq. (3) over the plate

TABLE III. Natural frequency parameters ($\lambda = 4l^2\omega\sqrt{\rho_e h/L}$) for one clamped, one simply supported, and two neighboring free edges (*C-SS-F-F*), ($\nu = 0.3$).

Frequency sequence	Leissa[30]	Present results		
		$M = N = 10$	$M = N = 15$	$M = N = 20$
1	6.9309	6.9094	6.9133	6.9148
2	27.289	27.142	27.159	27.166
3	38.586	38.391	38.384	38.384
4	64.254	63.985	64.001	64.011
5	67.467	67.227	67.194	67.188
6	108.02	107.70	107.69	107.70

must be zero because $\partial\phi/\partial n = 0$ on all other boundaries. This means that the mean of the deflection w must be zero. This condition is not always necessary or is not met for a plate in the vacuum. Therefore, these two cases are not identical. Also, physically, when ρ is very small, the liquid may not be treated as incompressible. If we include the compressibility effect at small ρ, for example, through the wave equation $\nabla^2\Phi - \Phi_{tt}/c^2 = 0$, where c is the speed of sound in the liquid, then these two cases do become identical. In fact, by substituting Eq. (8) into the wave equation, we can have $k_{mn}^2 = a_m^2 + b_n^2 - \omega^2/c^2$. Then, equations in Appendixes will become for a plate in the vacuum when $\rho \to 0$.

B. Natural frequencies of the coupled fluid-elasticity system

We now consider the case of liquid in the container with an elastic cover. The natural frequencies are calculated based on the solution procedures developed in Sec. II. In the following calculation, dimensionless variables are used based on three characteristic variables, namely, the half-length l, the density of liquid ρ, and the acceleration due to gravity g. Based on their combinations, all parameters mentioned below are nondimensionalised with an asterisk as its superscript, or $b^* = b/l$, $H^* = H/l$, $m^* = \rho_e h/(\rho l)$, $L^* = \frac{L}{\rho g l^4}$, and $\omega^* = \omega\sqrt{l/g}$.

We consider the effect of different ratios of b/l on the natural frequencies at different edge conditions. The natural frequencies ω^* corresponding to different values of b^* are provided in Tables IV–VI for completely clamped edges (*C-C-C-C*), completely free edges (*F-F-F-F*), and completely simply supported edges (*SS-SS-SS-SS*), respectively. They are arranged in the ascending order of ω^*. Further to the previous analysis, we have marked the group which each natural frequency belongs to in Tables IV–VI. The results for different combinations of these three conventional edge conditions can be obtained in a similar way.

For the free surface sloshing problem in a 3D rectangular tank, the modes at different m or n are fully uncoupled, and natural frequencies can be easily obtained from $\omega_{mn}^2 = gk_{mn}\tanh(k_{mn}H)$, $m, n = 0, 1, 2, \ldots$. In general, $\omega_{mn} \neq \omega_{nm}$ when $n \neq m$. However, they become the same frequency when $l = b$. This means that swapping n and m, or swapping the wave patterns in x and y will give the same frequency. When there is a plate on the top of the liquid, the modes at different m and n are not fully uncoupled. However, swapping the patterns in the x and y directions of a square tank still give the same frequency if the edge conditions on four sides are same. Mathematically, in S-S and A-A groups discussed previously, c and d can be simply swapped. In A-S, when c and d are swapped, it becomes S–A. This means that we can swap the deflection patterns in the x and y directions, and they give the same natural frequency, as can be seen in the following tables.

In Table IV, we can observe that for each column corresponding to mode sequence i ($i = 1 \sim 6$), the natural frequencies will decrease as the increase in b^*. This is similar to the trend of a rectangular plate in vacuum, shown in Table C1 in Leissa[30] for the same edge condition. However, we may find for *F-F-F-F* and *SS-SS-SS-SS*, this trend may not be followed in our results shown in Tables V and VI. These are different from the observation in Tables C15 and A1 in Leissa[30] for the same edge conditions where this trend still remains for a rectangular plate in vacuum.

For the vibration of a completely simply supported plate (*SS-SS-SS-SS*) without fluid, as the edge condition is symmetric about $y = 0$,

TABLE IV. Natural frequencies ω^* at different b^* with completely clamped edges *C-C-C-C*. ($m^* = 0.001, L^* = 0.1, H^* = 1, \nu = 0.3$).

| | ω^* | | | | | |
b^*	1	2	3	4	5	6
1/2	16.0994(A–S)	28.6810(S–S)	43.9108(S–A)	47.7197(A–S)	52.6813(A–A)	67.5184(S–A)
2/3	11.8108(A–S)	22.3649(S–A)	23.1988(S–S)	30.2318(A–A)	41.7875(A–S)	43.7442(S–A)
1	9.1023(S–A)	9.1023(A–S)	16.2526(A–A)	18.4141(S–S)	21.5904(S–S)	28.4469(S–A)
3/2	4.1779(S–A)	8.0426(A–S)	8.4907(S–S)	10.9605(A–A)	15.1390(S–A)	15.9108(A–S)
2	2.6628(S–A)	5.1360(S–S)	7.6821(A–S)	8.4637(S–A)	9.2951(A–A)	11.9837(A–S)

TABLE V. Natural frequencies ω^* at different b^* with completely free edges *F-F-F-F* ($m^* = 0.001, L^* = 0.1, H^* = 1, \nu = 0.3$).

| | ω^* | | | | | |
b^*	1	2	3	4	5	6
1/2	1.2002(A–S)	1.5010(A–S)	1.6934(S–A)	2.4870(A–S)	3.0521(A–A)	3.1625(S–S)
2/3	1.2010(A–S)	1.5037(A–S)	1.5076(S–A)	2.5184(A–S)	2.6080(A–A)	3.0194(S–A)
1	1.2022(S–A)	1.2022(A–S)	1.5079(S–A)	1.5079(A–S)	2.2786(A–A)	2.4421(A–A)
3/2	0.9059(S–A)	0.9537(S–A)	1.2032(A–S)	1.5116(A–S)	1.6891(A–A)	1.8050(S–S)
2	0.7197(S–A)	0.7302(S–A)	1.2038(A–S)	1.3170(S–S)	1.4693(A–A)	1.5081(S–S)

TABLE VI. Natural frequencies ω^* at different b^* with completely simply supported edges *SS-SS-SS-SS*. ($m^* = 0.001, L^* = 0.1, H^* = 1, \nu = 0.3$).

| | ω^* | | | | | |
b^*	1	2	3	4	5	6
1/2	1.4977(S–A)	1.5060(A–A)	1.5218(S–S)	1.9596(A–S)	4.7899(S–S)	5.1958(S–A)
2/3	1.1241(A–A)	1.1493(S–A)	1.6721(S–S)	1.9572(A–S)	2.3616(S–A)	3.6550(A–A)
1	1.0193(A–A)	1.5558(S–S)	1.8619(A–A)	1.9808(S–A)	1.9808(A–S)	3.2982(A–A)
3/2	1.3514(S–A)	2.0377(A–S)	2.5319(A–A)	3.1297(S–S)	3.9334(A–S)	5.9092(S–A)
2	0.9216(S–A)	1.9329(A–S)	1.9905(S–S)	2.2986(A–A)	2.7888(A–S)	3.1103(S–A)

it is expected to have both *y*-symmetric and *y*-antisymmetric deflection modes at different natural frequencies. For the *y*-antisymmetric modes, the corresponding natural frequencies will also be the natural frequencies of a *SS-SS-SS-SS* plate with the same length *l* but half width $b/2$. This has been pointed out in Leissa,[30] and the reason provided is that a simply supported condition is, in fact, satisfied along $y = 0$ in such a case. However, we find that it may be not applicable here. From Table VI, we can find that there is no such a relationship between results of $b^* = 1/2$ and $b^* = 1$, and results $b^* = 1$ and $b^* = 2$. This is, of course, due to the coupling with of liquid and the sidewall effects. For the *y*-antisymmetric case, for the potential, it is equivalent to the Dirichlet boundary condition $\phi = 0$ imposed on $y = 0$, which is different from the impermeable condition $\partial \phi / \partial n = 0$.

IV. MODE SHAPES

Once natural frequencies have been determined, the corresponding natural mode shapes can be further obtained. Using Eqs. (13), (15), (17), and (18), Eq. (16) yields

$$w(x, y) = \sum_{n=0}^{\infty} \sum_{m=0}^{\infty} I_{mn} \cos a_m(x + l) \cos b_n(y + b), \quad (32)$$

where

$$I_{mn} = C_{mn} + \sum_{i=1}^{4} \mu_m^{(i)} d_n^{(i)} + \sum_{i=1}^{4} \mu_n^{(i)} c_m^{(i)}$$

$$= \sum_{i=1}^{4} \left(\beta_{mn}^{(i)} + \mu_m^{(i)} S_{mn} \right) T_{mn} d_n^{(i)} + \sum_{i=1}^{4} \left(\alpha_{mn}^{(i)} + \mu_n^{(i)} S_{mn} \right) T_{mn} c_m^{(i)}, \quad (33)$$

and

$$T_{mn} = \frac{k_{mn} \tanh k_{mn} H}{k_{mn} S_{mn} \tanh k_{mn} H + \rho \omega^2}.$$

At a natural frequency, ω^*, when one of the non-zero deflection components $I_{m'n'}$ has been prescribed, the other I_{mn} and the deflection w

21 August 2024 09:24:30

at each point (x, y) can be further calculated. Specifically, for completely clamped, free or simply supported edge cases, based on the natural mode groups (S-S, A-S, S-A, and A-A) to which the natural frequency belongs to, we may prescribe I_{02} (as I_{00} is always zero), I_{10}, I_{01}, or I_{11}, respectively, to work out other corresponding $I_{2m,2n}$, $I_{2m+1,2n}$, $I_{2m,2n+1}$, or $I_{2m+1,2n+1}$ terms, while the remaining I_{mn} terms of other mode groups are zero. When the equation of prescribing a particular I_{mn} becomes linearly dependent to the existing ones, we may also prescribe $c_0^{(2)}$, $c_0^{(1)}$, $c_1^{(2)}$, and $c_1^{(1)}$, respectively, for natural mode groups S-S, A-S, S-A, and A-A.

In Fig. 2, the normalized mode shapes, or $z^* = w^*/\max[w^*]$, corresponding to the first six lowest natural frequencies are displayed for a square container covered by a clamped square plate. Based on the previous analysis, we have also marked the natural mode groups that the natural frequencies belong to. From the graphs, we can observe that the mode shapes are consistent with what is expected for the symmetry and anti-symmetry analysis. For a square tank, the S-A and A-S modes, such as displayed in Figs. 2(a) and 2(b), respectively, have the same natural frequencies, and their mode shapes become identical by rotating one of them to 90 degrees in the clockwise or counterclockwise direction. In addition, for different natural modes in the same mode group such as S-A, by comparing Figs. 2(a) and 2(f), we can observe that the mode shape becomes more complex with the increase in the natural frequency. This is consistent with the observation in Ren *et al.*[26] for a circular tank, where further discussion has been provided.

Similarly, we display the normalized mode shapes of the first six lowest natural frequencies of free edges (F-F-F-F) in Fig. 3. As there is no condition imposed on the deflection and slope at the edges, the mode shapes are expected to be quite different from those for clamped edges shown in Fig. 2. We can observe that the two mode shapes shown in Figs. 3(a) and 3(b) belong to S–A and A–S modes, respectively, which correspond to a same natural frequency as explained previously. Similar pattern is also shown in Figs. 3(c) and 3(d). However, major differences exist in the shape patterns shown in Figs. 3(a) and 3(c). For example, the mode shapes in Figs. 3(c) and 3(d) are more curved than those in Figs. 3(a) and 3(b). Numerical results also show that different from Figs. 3(c) and 3(d) where the maxima of the deflection are located at the corners, in Figs. 3(a) and 3(b), they are located, respectively, at the middle of the edges. Moreover, the mode shapes shown in Figs. 3(e) and 3(f) are all A–A modes, and the two corresponding nodal lines (where deflection is always zero during the vibration) are all straight ones along the x- and y-axes. This can be also observed from the result of I_{mn}. Based on the previous analysis, in A-A modes, only $I_{2m+1,2n+1}$ may not be zero, and then as $\cos(2m+1)\pi/2 = 0$ and $\cos(2n+1)\pi/2 = 0$, it gives $w(0, y) = w(x, 0) = 0$.

In addition, for a square tank covered by a plate of the same edge conditions, it is also observed that some mode shapes have symmetry or anti-symmetry feature with respect to the diagonal line. For example, both Fig. 3(e) and 3(f) belong to the A-A mode group, but are diagonally symmetric, or $w(-y, -x) = w(x, y)$, and anti-symmetric, or $w(-y, -x) = -w(x, y)$, respectively. This can also be seen from the result of $I_{2m+1,2n+1}$ $(m, n = 0, 1, 2, \ldots)$. $I_{2m+1,2n+1} = I_{2n+1,2m+1}$ $(c_n = d_n, n = 0, 1, 2\ldots)$ gives diagonally symmetric modes, while $I_{2m+1,2n+1} = -I_{2n+1,2m+1}$ $(c_n = -d_n, n = 0, 1, 2\ldots)$ gives diagonally anti-symmetric modes. When $b \neq l$, the mode shapes are shown in

Fig. 4 for a plate with completely clamped edges (C-C-C-C). There is no longer diagonal symmetry or anti-symmetry.

V. PRINCIPAL STRAIN

The principal strain of the rectangular plate cover can be calculated as the eigenvalues of the following strain tensor matrix:

$$\boldsymbol{\varepsilon} = -\frac{h}{2}\begin{bmatrix} W_{xx} & W_{xy} \\ W_{xy} & W_{yy} \end{bmatrix}, \tag{34}$$

or the solution of $\det[\boldsymbol{\varepsilon} - \lambda \boldsymbol{I}_2] = 0$, where $\boldsymbol{I}_2$ is the identity matrix of size 2. It further yields

$$\lambda_{1,2}(x, y, t) = -\frac{h\cos\omega t}{4}\left[w_{xx} + w_{yy} \pm \sqrt{(w_{xx} - w_{yy})^2 + 4w_{xy}^2}\right], \tag{35}$$

given that w is real and, thus, $W = \text{Re}\{w(x, y) \times e^{-i\omega t}\} = w\cos\omega t$. For each position (x, y), the maximum of the principal values $\lambda_{max}(x, y)$ can be obtained as $\max\left\{\left|\frac{\lambda_1}{\cos\omega t}\right|, \left|\frac{\lambda_2}{\cos\omega t}\right|\right\}$, or $\lambda_{max}(x, y) = \frac{h}{4}\left[|w_{xx} + w_{yy}| + \sqrt{(w_{xx} - w_{yy})^2 + 4w_{xy}^2}\right]$. A similar procedure can be found in Ren *et al.*[26] for an upright circular cylindrical tank with an elastic cover. In Fig. 5, we display the maximal principal strain at different positions on the elastic cover with completely clamped edges in a non-square tank at different natural modes corresponding to the cases shown in Fig. 4. From the figure, we can observe that when the mode shape becomes more oscillatory, the maximum principal strain tends to more oscillatory as well. For the clamped edge case, the peaks of the maximum principal strain occur on the edge, which is consistent with the observation in the rectangular channel.[28]

VI. CONCLUSIONS

An efficient solution scheme has been developed to investigate the coupled free vibrations of liquid in a three-dimensional rectangular container covered by an elastic cover. This scheme is applicable for any combinations of edge conditions. Examples are provided for the three most common ones, namely, clamped, free edge, and simply supported.

When $\rho \to 0$, the results are not always identical to that when $\rho = 0$. This is due to the assumption of the incompressible liquid, which may not be valid as $\rho \to 0$. When the compressibility effect is included through replacing the Laplace equation with the wave equation, these two cases of $\rho \to 0$ and $\rho = 0$ become identical.

When the cover has the same edge type on its four sides, the entire coefficient matrix can be split into four independent block matrices, from which four groups of natural frequencies can be obtained. Correspondingly, the natural modes can be split into four mode groups, which are uncoupled from each other, with mode shapes either symmetric (S) or antisymmetric (A) with respect to the longitudinal and transverse directions, respectively. For a square tank, the S-A and A-S modes share the same natural frequencies, and their mode shapes could be mutually converted through rotating the tank in a clockwise or counterclockwise direction by 90 degrees.
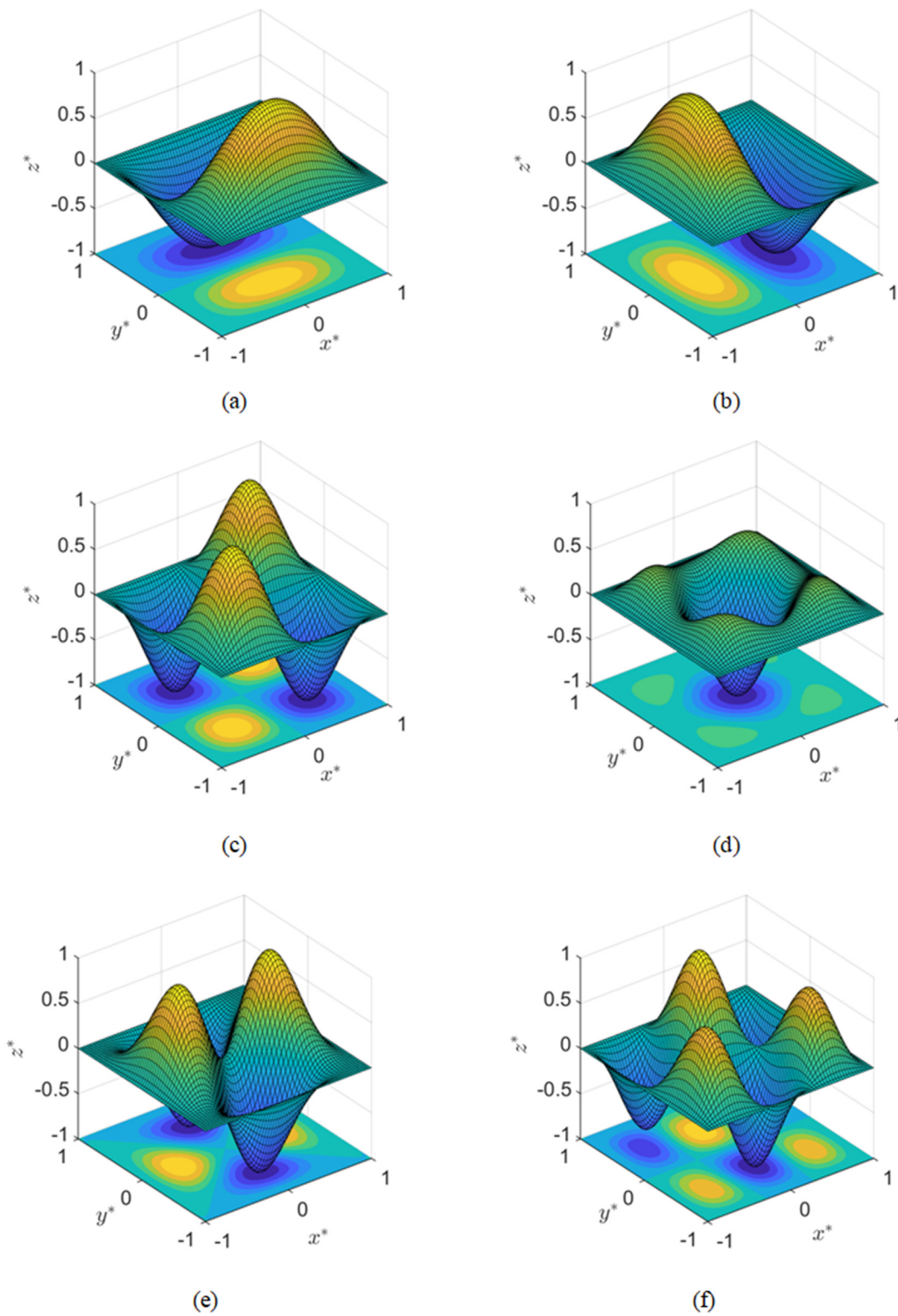
21 August 2024 09:24:30

FIG. 2. Normalized mode shapes with clamped edges (C-C-C-C) in a square tank: $b^* = 1, m^* = 0.001, L^* = 0.1, H^* = 1$, and $\nu = 0.3$. (a) $\omega^* = 9.1023$ (S-A); (b) $\omega^* = 9.1023$ (A-S); (c) $\omega^* = 16.2526$ (A-A); (d) $\omega^* = 18.4141$ (S-S); (e) $\omega^* = 21.5904$ (S-S); (f) $\omega^* = 28.4469$ (S-A).
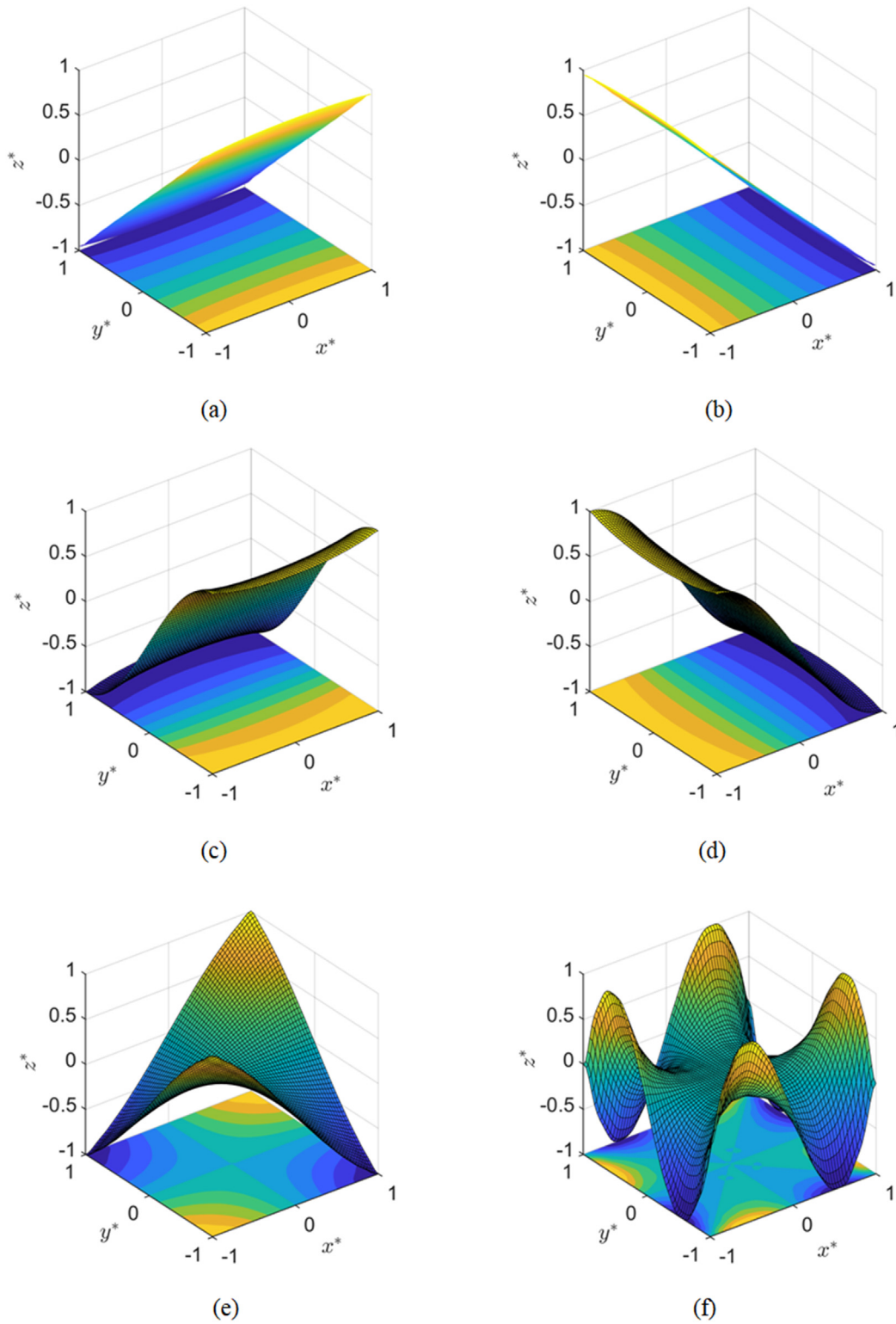
21 August 2024 09:24:30

FIG. 3. Normalized mode shapes with completely free edges in a square tank: $b^* = 1$, $m^* = 0.001$, $L^* = 0.1$, $H^* = 1$, and $\nu = 0.3$.(a) $\omega^* = 1.2022$ (S–A); (b) $\omega^* = 1.2022$ (A–S); (c) $\omega^* = 1.5079$ (S–A); (d) $\omega^* = 1.5079$ (A–S); (e) $\omega^* = 2.2786$ (A–A); (f) $\omega^* = 2.4421$ (A–A).
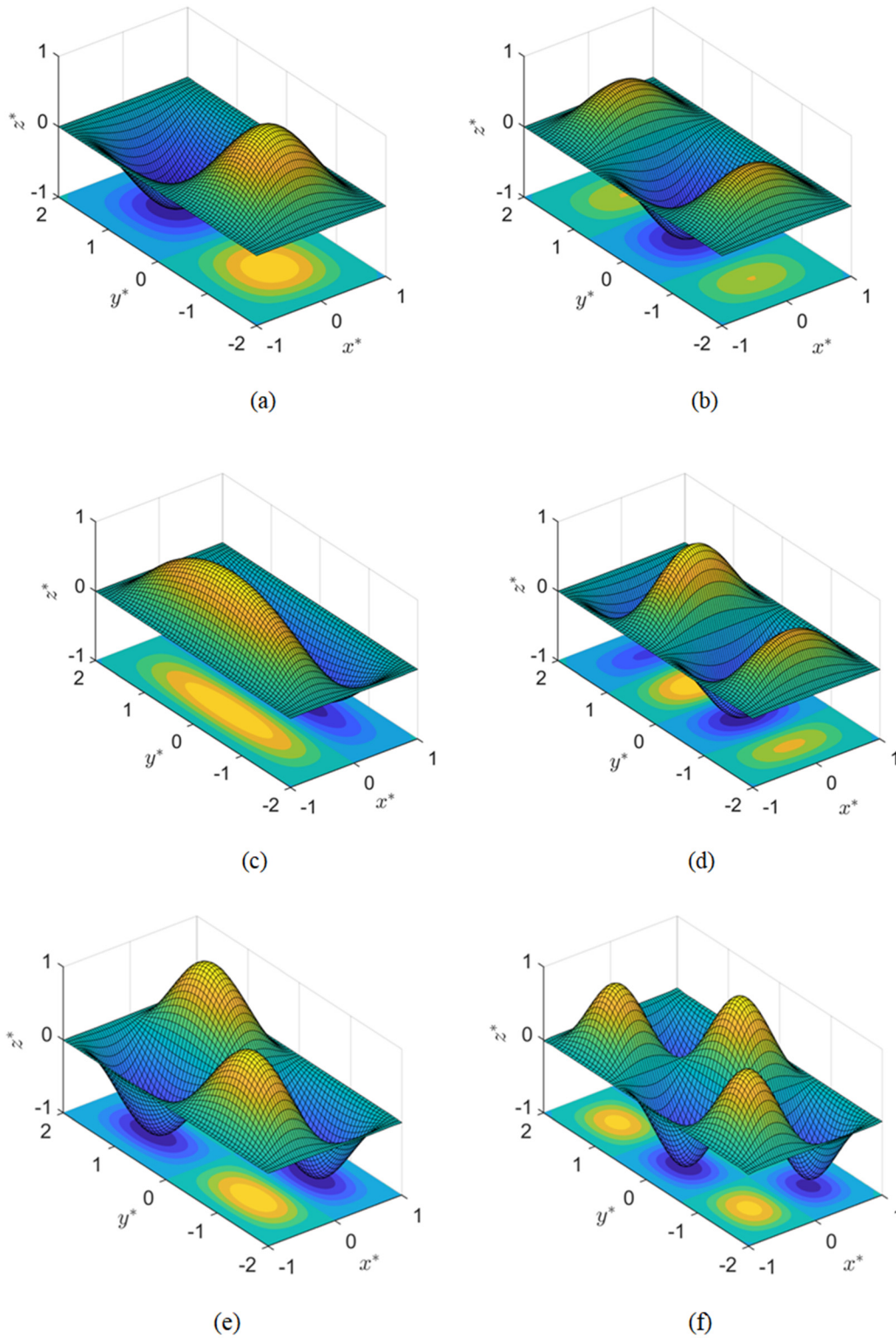
21 August 2024 09:24:30

FIG. 4. Normalized mode shapes with completely clamped edges in a non-square tank: $b^* = 2$, $m^* = 0.001$, $L^* = 0.1$, $H^* = 1$, and $\nu = 0.3$. (a) $\omega^* = 2.6628$(S-A); (b) $\omega^* = 5.1360$ (S-S); (c) $\omega^* = 7.6821$ (A-S); (d) $\omega^* = 8.4637$(S-A); and (e) $\omega^* = 9.2951$(A-A); (f) $\omega^* = 11.9837$ (A-S).
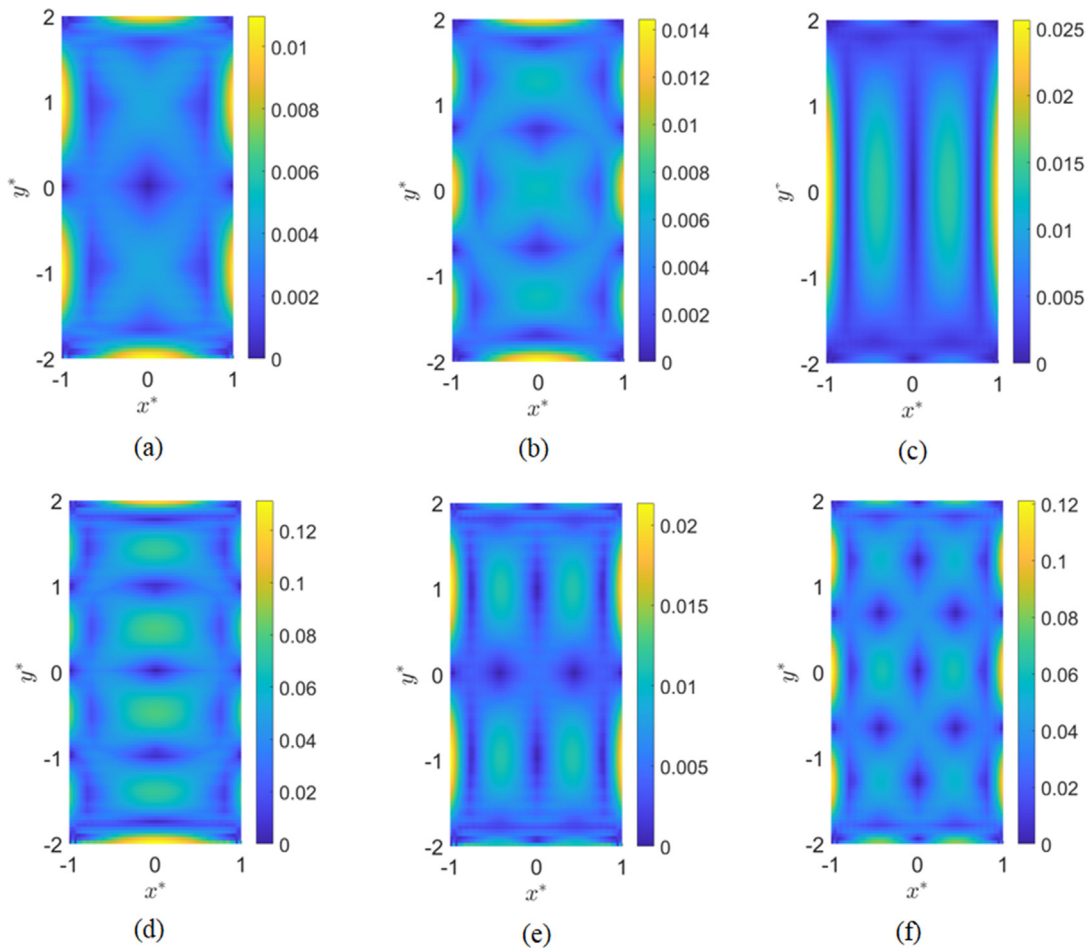
21 August 2024 09:24:30

FIG. 5. Maximal principal strain distribution on the elastic cover with completely clamped edges (C-C-C-C): $b^* = 2$, $h^* = 0.001$, $m^* = 0.001$, $L^* = 0.1$, $H^* = 1$, and $\nu = 0.3$. (a) $\omega^* = 2.6628$(S-A) at $l_{01}^* = 1$; (b) $\omega^* = 5.1360$(S-S) at $l_{02}^* = 1$; (c) $\omega^* = 7.6821$ (A–S) at $l_{10}^* = 1$; (d) $\omega^* = 8.4637$(S–A) at $l_{01}^* = 1$; (e) $\omega^* = 9.2951$(A–A) at $l_{11}^* = 1$; (f) $\omega^* = 11.9837$ (A–S) at $l_{10}^* = 1$.

The effect of aspect ratios of the tank on natural frequencies is investigated through various b/l. It is observed that for the elastic cover with completely clamped edges, the present results show a similar trend with those of a rectangular cover in vacuum. However, for the completely free or completely simply supported case, due to the effect of the tank walls and fluid, the trends will no longer be the same as those of a rectangular cover in vacuum.

For different natural modes in each mode group, it is observed that both the graphs of mode shape and the maximum principal strain become more oscillatory with the increase in natural frequencies. The peaks of the maximum principal strain occur at the side walls for completely clamped edge case.

ACKNOWLEDGMENTS

AUTHOR DECLARATIONS
Conflict of Interest

The authors have no conflicts to disclose.

Author Contributions

K. Ren: Conceptualization (supporting); data curation (lead); methodology (equal); software (lead); visualization (lead); writing – original draft (lead); writing – review and editing (equal). **G. X. Wu:** Conceptualization (lead); methodology (equal); supervision (lead); writing – original draft (supporting); writing – review and editing (equal). **Y. F. Yang:** Writing – original draft (supporting); writing – review and editing (supporting).

DATA AVAILABILITY

The data that support the findings of this study are available within the article.

21 August 2024 09:24:30

APPENDIX A: LINEAR EQUATIONS FOR COMPLETELY CLAMPED EDGES CASE

From $w(x = -l) = 0$

$$\sum_{i=1}^{4} \underbrace{\sum_{m=0}^{\infty} \left(\mu_m^{(i)} S_{mn} + \beta_{mn}^{(i)} \right) T_{mn} d_n^{(i)}}_{A_{1i}}$$
$$= -\sum_{m=0}^{\infty} \sum_{i=1}^{4} \left(\mu_n^{(i)} S_{mn} + \alpha_{mn}^{(i)} \right) T_{mn} c_m^{(i)}, \quad (n = 0, 1, 2, \ldots). \quad (A1)$$

From $w(x = l) = 0$

$$\sum_{i=1}^{4} \underbrace{\sum_{m=0}^{\infty} \left(\mu_m^{(i)} S_{mn} + \beta_{mn}^{(i)} \right) T_{mn} (-1)^m d_n^{(i)}}_{A_{2i}}$$
$$= -\sum_{m=0}^{\infty} \sum_{i=1}^{4} \left(\mu_n^{(i)} S_{mn} + \alpha_{mn}^{(i)} \right) T_{mn} (-1)^m c_m^{(i)}, \quad (n = 0, 1, 2, \ldots). \quad (A2)$$

From $w(y = -b) = 0$

$$\sum_{i=1}^{4} \underbrace{\sum_{n=0}^{\infty} \left(\mu_n^{(i)} S_{mn} + \alpha_{mn}^{(i)} \right) T_{mn} c_m^{(i)}}_{B_{1i}}$$
$$= -\sum_{n=0}^{\infty} \sum_{i=1}^{4} \left(\mu_m^{(i)} S_{mn} + \beta_{mn}^{(i)} \right) T_{mn} d_n^{(i)}, \quad (m = 0, 1, 2, \ldots). \quad (A3)$$

From $w(y = b) = 0$

$$\sum_{i=1}^{4} \underbrace{\sum_{n=0}^{\infty} \left(\mu_n^{(i)} S_{mn} + \alpha_{mn}^{(i)} \right) T_{mn} (-1)^n c_m^{(i)}}_{B_{2i}}$$
$$= -\sum_{n=0}^{\infty} \sum_{i=1}^{4} \left(\mu_m^{(i)} S_{mn} + \beta_{mn}^{(i)} \right) T_{mn} (-1)^n d_n^{(i)}, \quad (m = 0, 1, 2, \ldots). \quad (A4)$$

From $w_x(x = -l) = 0$

$$\sum_{i=1}^{4} i \times (-1)^{i-1} \times d_n^{(i)} = 0, \quad (n = 0, 1, 2, \ldots). \quad (A5)$$

From $w_x(x = l) = 0$

$$\sum_{i=1}^{4} i \times d_n^{(i)} = 0, \quad (n = 0, 1, 2, \ldots). \quad (A6)$$

From $w_y(y = -b) = 0$

$$\sum_{i=1}^{4} i \times (-1)^{i-1} \times c_m^{(i)} = 0, \quad (m = 0, 1, 2, \ldots). \quad (A7)$$

From $w_y(y = b) = 0$

$$\sum_{i=1}^{4} i \times c_m^{(i)} = 0. \quad (m = 0, 1, 2, \ldots). \quad (A8)$$

Through (A1) $\pm$ (A2) and (A5) $\pm$ (A6), and using $\mu_{2n}^{(1)} = \mu_{2n}^{(3)} = 0$ and $\mu_{2n+1}^{(2)} = \mu_{2n+1}^{(4)} = 0$, we can obtain

$$d_n^{(1)} = \frac{Y_1}{\left(2A_{11} - \frac{2}{3} A_{13} \right)}; \quad d_n^{(3)} = -\frac{d_n^{(1)}}{3},$$

$$d_n^{(2)} = \frac{Y_2}{(2A_{12} - A_{14})}; \quad d_n^{(4)} = -\frac{d_n^{(2)}}{2},$$

where Y_1 has only c_{2m+1} terms and Y_2 has only c_{2m} terms.

Through (A3) $\pm$ (A4) and (A7) $\pm$ (A8), we can write c_m in terms of d_n in a similar way as

$$c_m^{(1)} = \frac{X_1}{\left(2B_{11} - \frac{2}{3} B_{13} \right)}; \quad c_m^{(3)} = -\frac{c_m^{(1)}}{3},$$

$$c_m^{(2)} = \frac{X_2}{(2B_{12} - B_{14})}; \quad c_m^{(4)} = -\frac{c_m^{(2)}}{2},$$

where X_1 has only d_{2n+1} terms and X_2 has only d_{2n} terms. Then, we put d_n into X_1 and X_2, and we can split all the unknowns of c_m into four groups, namely, $c_{2m}^{(2i)}, c_{2m}^{(2i-1)}, c_{2m+1}^{(2i)}$, and $c_{2m+1}^{(2i-1)}$ ($i = 1, 2; m = 0, 1, 2 \ldots$). Similarly, we can also split $d_n^{(i)}$ into four groups as $d_{2n}^{(2i)}, d_{2n}^{(2i-1)}, d_{2n+1}^{(2i)}$, and $d_{2n+1}^{(2i-1)}$ ($i = 1, 2; n = 0, 1, 2 \ldots$). Then, the unknowns can be split into four fully independent groups, namely, (a) $c_{2m}^{(2i)}, d_{2n}^{(2i)}$, (b) $c_{2m}^{(2i-1)}, d_{2n+1}^{(2i)}$, (c) $c_{2m+1}^{(2i)}, d_{2n}^{(2i-1)}$, and (d) $c_{2m+1}^{(2i-1)}, d_{2n+1}^{(2i-1)}$, while within each group, the unknowns are coupled.

APPENDIX B: LINEAR EQUATIONS FOR COMPLETELY FREE EDGES

From $\left[\frac{\partial^2 w}{\partial x^2} + \nu \frac{\partial^2 w}{\partial y^2} \right]_{x=-l} = 0$

$$-\sum_{m=0}^{\infty} \sum_{i=1}^{4} \left\{ \left(a_m^2 + \nu b_n^2 \right) \times \frac{\alpha_{mn}^{(i)} k_{mn} \tanh k_{mn} H - \rho \omega^2 \mu_n^{(i)}}{k_{mn} S_{mn} \tanh k_{mn} H + \rho \omega^2} \right.$$
$$\left. + \left(a_m^2 \mu_n^{(i)} - \frac{\nu (i-1) i \mu_n^{(i-2)}}{b^2} \right) \right\} c_m^{(i)}$$
$$- \sum_{i=1}^{4} \left\{ \sum_{m=0}^{\infty} \left(a_m^2 + \nu b_n^2 \right) \times \frac{\beta_{mn}^{(i)} k_{mn} \tanh k_{mn} H - \rho \omega^2 \mu_m^{(i)}}{k_{mn} S_{mn} \tanh k_{mn} H + \rho \omega^2} \right.$$
$$\left. + (-1)^{i+1} \left(-\nu b_n^2 + \frac{(i-1) i}{l^2} \right) \right\} d_n^{(i)} = 0 \quad (n = 0, 1, 2, \ldots). \quad (B1)$$

From $\left[\frac{\partial^2 w}{\partial x^2} + \nu \frac{\partial^2 w}{\partial y^2} \right]_{x=l} = 0$

$$-\sum_{m=0}^{\infty}\sum_{i=1}^{4}(-1)^{m}\left\{\left(a_m^2+\nu b_n^2\right)\times\frac{\alpha_{mn}^{(i)}k_{mn}\tanh k_{mn}H-\rho\omega^2\mu_n^{(i)}}{k_{mn}S_{mn}\tanh k_{mn}H+\rho\omega^2}\right.$$
$$+\left.\left(a_m^2\mu_n^{(i)}-\frac{\nu(i-1)i\,\mu_n^{(i-2)}}{b^2}\right)\right\}c_m^{(i)}$$
$$-\sum_{i=1}^{4}\left\{\sum_{m=0}^{\infty}\left(a_m^2+\nu b_n^2\right)(-1)^m\times\frac{\beta_{mn}^{(i)}k_{mn}\tanh k_{mn}H-\rho\omega^2\mu_m^{(i)}}{k_{mn}S_{mn}\tanh k_{mn}H+\rho\omega^2}\right.$$
$$+\left.\left(\nu b_n^2-\frac{(i-1)i}{l^2}\right)\right\}d_n^{(i)}=0\quad(n=0,1,2,\ldots).\qquad(B2)$$

From $\left[\frac{\partial^2 w}{\partial y^2}+\nu\frac{\partial^2 w}{\partial x^2}\right]_{y=-b}=0$

$$-\sum_{i=1}^{4}\left\{\sum_{n=0}^{\infty}\left(\nu a_m^2+b_n^2\right)\times\frac{\alpha_{mn}^{(i)}k_{mn}\tanh k_{mn}H-\rho\omega^2\mu_n^{(i)}}{k_{mn}S_{mn}\tanh k_{mn}H+\rho\omega^2}\right.$$
$$+\left.(-1)^i\left(\nu a_m^2-\frac{(i-1)i}{b^2}\right)\right\}c_m^{(i)}$$
$$-\sum_{n=0}^{\infty}\sum_{i=1}^{4}\left\{\left(\nu a_m^2+b_n^2\right)\times\frac{\beta_{mn}^{(i)}k_{mn}\tanh k_{mn}H-\rho\omega^2\mu_m^{(i)}}{k_{mn}S_{mn}\tanh k_{mn}H+\rho\omega^2}\right.$$
$$+\left.\left(b_n^2\mu_m^{(i)}-\frac{\nu(i-1)i\,\mu_m^{(i-2)}}{l^2}\right)\right\}d_n^{(i)}=0\quad(m=0,1,2,\ldots).$$
$$(B3)$$

From $\left[\frac{\partial^2 w}{\partial y^2}+\nu\frac{\partial^2 w}{\partial x^2}\right]_{y=b}=0$

$$-\sum_{i=1}^{4}\left\{\sum_{n=0}^{\infty}\left(\nu a_m^2+b_n^2\right)(-1)^n\times\frac{\alpha_{mn}^{(i)}k_{mn}\tanh k_{mn}H-\rho\omega^2\mu_n^{(i)}}{k_{mn}S_{mn}\tanh k_{mn}H+\rho\omega^2}\right.$$
$$+\left.\left(\nu a_m^2-\frac{(i-1)i}{b^2}\right)\right\}c_m^{(i)}$$
$$-\sum_{n=0}^{\infty}\sum_{i=1}^{4}(-1)^n\left\{\left(\nu a_m^2+b_n^2\right)\times\frac{\beta_{mn}^{(i)}k_{mn}\tanh k_{mn}H-\rho\omega^2\mu_m^{(i)}}{k_{mn}S_{mn}\tanh k_{mn}H+\rho\omega^2}\right.$$
$$+\left.\left(b_n^2\mu_m^{(i)}-\frac{\nu(i-1)i\,\mu_m^{(i-2)}}{l^2}\right)\right\}d_n^{(i)}=0\quad(m=0,1,2,\ldots).$$
$$(B4)$$

From $\left[\frac{\partial^3 w}{\partial x^3}+(2-\nu)\frac{\partial^3 w}{\partial x\partial y^2}\right]_{x=-l}=0$

$$\sum_{i=1}^{4}\left(\frac{(2-\nu)b_n^2}{l}\times(-1)^i\times i+\frac{6\delta_{i3}}{l^3}-\frac{24\delta_{i4}}{l^3}\right)d_n^{(i)}=0$$
$$(n=0,1,2,\ldots).\qquad(B5)$$

From $\left[\frac{\partial^3 w}{\partial x^3}+(2-\nu)\frac{\partial^3 w}{\partial x\partial y^2}\right]_{x=l}=0$

$$\sum_{i=1}^{4}\left(-\frac{(2-\nu)b_n^2}{l}\times i+\frac{6\delta_{i3}}{l^3}+\frac{24\delta_{i4}}{l^3}\right)d_n^{(i)}=0\quad(n=0,1,2,\ldots).$$
$$(B6)$$

From $\left[\frac{\partial^3 w}{\partial y^3}+(2-\nu)\frac{\partial^3 w}{\partial y\partial x^2}\right]_{y=-b}=0$

$$\sum_{i=1}^{4}\left(\frac{(2-\nu)a_m^2}{b}\times(-1)^i\times i+\frac{6\delta_{i3}}{b^3}-\frac{24\delta_{i4}}{b^3}\right)c_m^{(i)}=0$$
$$(m=0,1,2,\ldots).\qquad(B7)$$

From $\left[\frac{\partial^3 w}{\partial y^3}+(2-\nu)\frac{\partial^3 w}{\partial y\partial x^2}\right]_{y=b}=0$

$$\sum_{i=1}^{4}\left(-\frac{(2-\nu)a_m^2}{b}\times i+\frac{6\delta_{i3}}{b^3}+\frac{24\delta_{i4}}{b^3}\right)c_m^{(i)}=0\quad(m=0,1,2,\ldots).$$
$$(B8)$$

REFERENCES

[1] B. W. Wilson, "Seiches", Adv. Hydrosci. **8**, 1–94 (1972).

[2] O. F. Rognebakke and O. M. Faltinsen, "Coupling of sloshing and ship motions," J. Ship Res. **47**, 208–221 (2003).

[3] S. Wu and Y. Ju, "Numerical study of the boil-off gas (BOG) generation characteristics in a type C independent liquefied natural gas (LNG) tank under sloshing excitation," Energy **223**, 120001 (2021).

[4] A. E. Veldman, J. Gerrits, R. Luppes, J. A. Helder, and J. P. B. Vreeburg, "The numerical simulation of liquid sloshing on board spacecraft," J. Comput. Phys. **224**, 82–99 (2007).

[5] C. Farhat, E. K. Y. Chiu, D. Amsallem, J. S. Schotté, and R. Ohayon, "Modeling of fuel sloshing and its physical effects on flutter," AIAA J. **51**, 2252–2265 (2013).

[6] S. M. Longshaw and B. D. Rogers, "Automotive fuel cell sloshing under temporally and spatially varying high acceleration using GPU-based Smoothed Particle Hydrodynamics (SPH)," Adv. Eng. Softw. **83**, 31–44 (2015).

[7] M. J. Smith, J. J. Kobine, and F. A. Davidson, "Free and forced motion in an asymmetric liquid-column oscillator," Proc. R. Soc. A **464**, 905–922 (2008).

[8] R. A. Ibrahim, *Liquid Sloshing Dynamics: Theory and Applications* (Cambridge University Press, Cambridge, 2005).

[9] O. M. Faltinsen and A. N. Timokha, *Sloshing* (Cambridge University Press, Cambridge, 2009).

[10] H. N. Abramson, "The dynamic behavior of liquids in moving containers," NASA, Report SP 106, 1966.

[11] G. X. Wu, Q. W. Ma, and R. E. Taylor, "Numerical simulation of sloshing waves in a 3D tank based on a finite element method," Appl. Ocean Res. **20**, 337–355 (1998).

[12] O. M. Faltinsen, O. F. Rognebakke, and A. N. Timokha, "Resonant three-dimensional nonlinear sloshing in a square-base basin," J. Fluid Mech. **487**, 1–42 (2003).

[13] D. Liu and P. Lin, "A numerical study of three-dimensional liquid sloshing in tanks," J. Comput. Phys. **227**, 3921–3939 (2008).

[14] P. A. Caron, M. A. Cruchaga, and A. E. Larreteguy, "Study of 3D sloshing in a vertical cylindrical tank," Phys. Fluids **30**, 082112 (2018).

[15] J. Núñez Aedo, M. Cruchaga, and E. Castillo del Barrio, "Study on the dependence with the filling level of the sloshing wave pattern in a rectangular tank," Phys. Fluids **32**, 012101 (2020).

[16] C. Zhang, X. Sun, P. Wang, L. Chen, and D. Ning, "Hydrodynamics of a floating liquid-tank barge adjacent to fixed structure in beam waves," Phys. Fluids **34**, 047114 (2022).

[17] N. G. Kuznetsov and O. V. Motygin, "Sloshing in vertical cylinders with circular walls: The effect of radial baffles," Phys. Fluids **33**, 102106 (2021).

[18] E. Hernández and D. Santamarina, "Active control of sloshing in containers with elastic baffle plates," Int. J. Numer. Meth. Eng. **91**, 604–621 (2012).

[19] S. M. Hasheminejad, M. M. Mohammadi, and A. Jamalpoor, "Hydroelastic modeling and active control of transient sloshing in a three dimensional rectangular floating roof tank," J. Sound Vib. **470**, 115146 (2020).

[20] Y. Xie and X. Zhao, "Sloshing suppression with active controlled baffles through deep reinforcement learning–expert demonstrations–behavior cloning process," Phys. Fluids **33**, 017115 (2021).

[21] H. F. Bauer, "Coupled frequencies of a liquid in a circular cylindrical container with elastic liquid surface cover," J. Sound Vib. **180**, 689–704 (1995).

[22]W. Parasil and N. Watanabe, "Nonlinear dynamic analysis of the interaction between a two-dimensional rubberlike membrane and a liquid in a rectangular tank," Aerosp. Sci. Technol. **56**, 212–222 (2016).

[23]H. F. Bauer and K. Komatsu, "Coupled frequencies of a frictionless liquid in a circular cylindrical tank with an elastic partial surface cover," J. Sound Vib. **230**, 1147–1163 (2000).

[24]Y. W. Kim and Y. S. Lee, "Coupled vibration analysis of liquid-filled rigid cylindrical storage tank with an annular plate cover," J. Sound Vib. **279**, 217–235 (2005).

[25]M. Amabili, "Vibrations of circular plates resting on a sloshing liquid: Solution of the fully coupled problem," J. Sound Vib **245**, 261–283 (2001).

[26]K. Ren, G. X. Wu, and Z. F. Li, "Natural modes of liquid sloshing in a cylindrical container with an elastic cover," J. Sound Vib **512**, 116390 (2021).

[27]T. Matsui, "Sloshing in a cylindrical liquid storage tank with a single-deck type floating roof under seismic excitation," ASME. J. Pressure Vessel Technol. **131**, 21303 (2009).

[28]K. Ren, G. X. Wu, and Z. F. Li, "Hydroelastic waves propagating in an ice-covered channel," J. Fluid Mech. **886**, A18 (2020).

[29]S. P. Timoshenko and S. Woinowsky-Krieger, *Theory of Plates and Shells* (McGraw-Hill, New York, 1959).

[30]A. W. Leissa, "The free vibration of rectangular plate," J. Sound Vib. **31**, 257–293 (1973).

[31]W. L. Li, X. Zhang, J. Du, and Z. Liu, "An exact series solution for the transverse vibration of rectangular plates with general elastic boundary supports," J. Sound Vib. **321**, 254–269 (2009).

21 August 2024 09:24:30